#### **NEUROPHYSIOLOGY**

# Synaptic zinc inhibition of NMDA receptors depends on the association of GluN2A with the zinc transporter ZnT1

Rebecca F. Krall<sup>1,2,3,4</sup>, Aubin Moutal<sup>5</sup>, Matthew B. Phillips<sup>6</sup>, Hila Asraf<sup>7</sup>, Jon W. Johnson<sup>6</sup>, Rajesh Khanna<sup>5</sup>, Michal Hershfinkel<sup>7</sup>, Elias Aizenman<sup>2,3,4,7</sup>\*, Thanos Tzounopoulos<sup>1,2,3</sup>\*

The NMDA receptor (NMDAR) is inhibited by synaptically released zinc. This inhibition is thought to be the result of zinc diffusion across the synaptic cleft and subsequent binding to the extracellular domain of the NMDAR. However, this model fails to incorporate the observed association of the highly zinc-sensitive NMDAR subunit GluN2A with the postsynaptic zinc transporter ZnT1, which moves intracellular zinc to the extracellular space. Here, we report that disruption of ZnT1-GluN2A association by a cell-permeant peptide strongly reduced NMDAR inhibition by synaptic zinc in mouse dorsal cochlear nucleus synapses. Moreover, synaptic zinc inhibition of NMDARs required postsynaptic intracellular zinc, suggesting that cytoplasmic zinc is transported by ZnT1 to the extracellular space in close proximity to the NMDAR. These results challenge a decades-old dogma on how zinc inhibits synaptic NMDARs and demonstrate that presynaptic release and a postsynaptic transporter organize zinc into distinct microdomains to modulate NMDAR neurotransmission.

Copyright © 2020
The Authors, some rights reserved; exclusive licensee American Association for the Advancement of Science. No claim to original U.S. Government Works. Distributed under a Creative Commons Attribution NonCommercial License 4.0 (CC BY-NC).

#### **INTRODUCTION**

Zinc is a neuromodulator that regulates glutamatergic,  $\gamma$ -aminobutyric acid-mediated (GABAergic), and glycinergic synaptic transmission (1–7); short- and long-term synaptic plasticity (2, 8–12); auditory processing; and acuity for sensory stimulus discrimination (13–15). The zinc transporter ZnT3 (Slc30a3) packages zinc into presynaptic vesicles of large populations of excitatory neurons in many brain regions, including the cerebral cortex, hippocampus, amygdala, and dorsal cochlear nucleus (DCN) (16). During synaptic activity, vesicular zinc is released from ZnT3-containing terminals (1, 17) and diffuses across the synaptic cleft (4) to modulate a number of postsynaptic receptors (3, 6, 18, 19), including the highly zinc-sensitive N-methyl-D-aspartate receptor (NMDAR) (2, 4, 20).

GluN2A-containing NMDARs are the major postsynaptic targets of synaptically released zinc due to their sensitivity to nanomolar concentrations of extracellular zinc, which inhibit receptor function (20). It is generally accepted that zinc release alone provides sufficient accumulation of the metal in the synaptic cleft to account for the observed zinc inhibition of GluN2A-containing NMDARs (2, 4, 9). However, this model only considers ZnT3's contribution to activity-dependent vesicular zinc inhibition of NMDARs when there are 24 known unique zinc transporters (10 Slc30a and 14 Slc39a) (21) that may be involved in zinc's spatial distribution in synapses. Little is known, however, how zinc transporters other than ZnT3 influence synaptic zinc's actions upon its receptor targets.

<sup>1</sup>Department of Otolaryngology, University of Pittsburgh School of Medicine, Pittsburgh, PA 15261, USA. <sup>2</sup>Pittsburgh Hearing Research Center, University of Pittsburgh School of Medicine, Pittsburgh, PA 15261, USA. <sup>3</sup>Department of Neurobiology, University of Pittsburgh School of Medicine, Pittsburgh, PA 15261, USA. <sup>4</sup>Pittsburgh Institute for Neurodegenerative Diseases, University of Pittsburgh School of Medicine, Pittsburgh, PA 15261, USA. <sup>5</sup>Department of Pharmacology, College of Medicine, University of Arizona, Tucson, AZ 85724, USA. <sup>6</sup>Department of Neuroscience, University of Pittsburgh, Pittsburgh, PA 15261, USA. <sup>7</sup>Department of Physiology and Cell Biology, Ben-Gurion University of the Negev, Faculty of Health Sciences, Beer-Sheva, Israel.

ZnT1 (Slc30a1), a cell membrane transporter that shuttles zinc from the cytoplasm to the extracellular space, not only localizes to the postsynaptic density (22) but also binds directly to the GluN2A subunit of NMDARs (23). This positions ZnT1, in concert with the presynaptic ZnT3 transporter, as a likely co-regulator of synaptic zinc concentration and function in the synaptic cleft. Here, we developed a cell-permeant peptide to disrupt ZnT1-GluN2A binding and used ZnT3 null mice and zinc chelation to assess the contribution of ZnT1 into synaptic actions of zinc. Our studies reveal a previously unknown interplay between ZnT3- and ZnT1-dependent zinc transport to inhibit NMDAR-mediated neurotransmission.

#### **RESULTS**

#### N2AZ disrupts the binding of ZnT1 to GluN2A

To study the effects of ZnT1 on zinc inhibition of NMDARs, we designed a cell-permeant peptide aimed at disrupting the ZnT1-GluN2A interaction. First, we constructed a peptide spot array spanning 74 amino acids of the C-terminal domain (residues 1390 to 1464) of mouse GluN2A (UniProt no.: P35436), previously shown to be necessary for ZnT1-GluN2A binding (23). The array consisted of sixty-one 15-mers, each sequentially overlapping by 14 amino acids, similar to procedures described earlier by our groups for other protein-protein interaction systems (24, 25). Next, we probed the peptide spot arrays with Flag-tagged ZnT1-enriched human embryonic kidney (HEK) cell lysates and then visualized and quantified ZnT1 binding with immunofluorescence against the Flag tag (Fig. 1A). This approach identified three regions of ZnT1 binding, spanning peptide numbers 2 to 8, 40 to 42, and 48 to 52 in Fig. 1 (A and B). We focused on the broadest binding peak (peptides 2 to 8; Fig. 1B, in red), which included a common nine-amino acid sequence among the peptides with high ZnT1 binding (NDSYLRSSL, corresponding to GluN2A residues 1397 to 1406). This nine-amino acid sequence is conserved in mouse, rat, and human GluN2A sequences (isoform 1; UniProt no.: rat, Q00959; human, Q12879). Last, this peptide and a scrambled control (SNLSDSYLR; Fig. 1B,

<sup>\*</sup>Corresponding author. Email: redox@pitt.edu (E.A.); thanos@pitt.edu (T.T.)

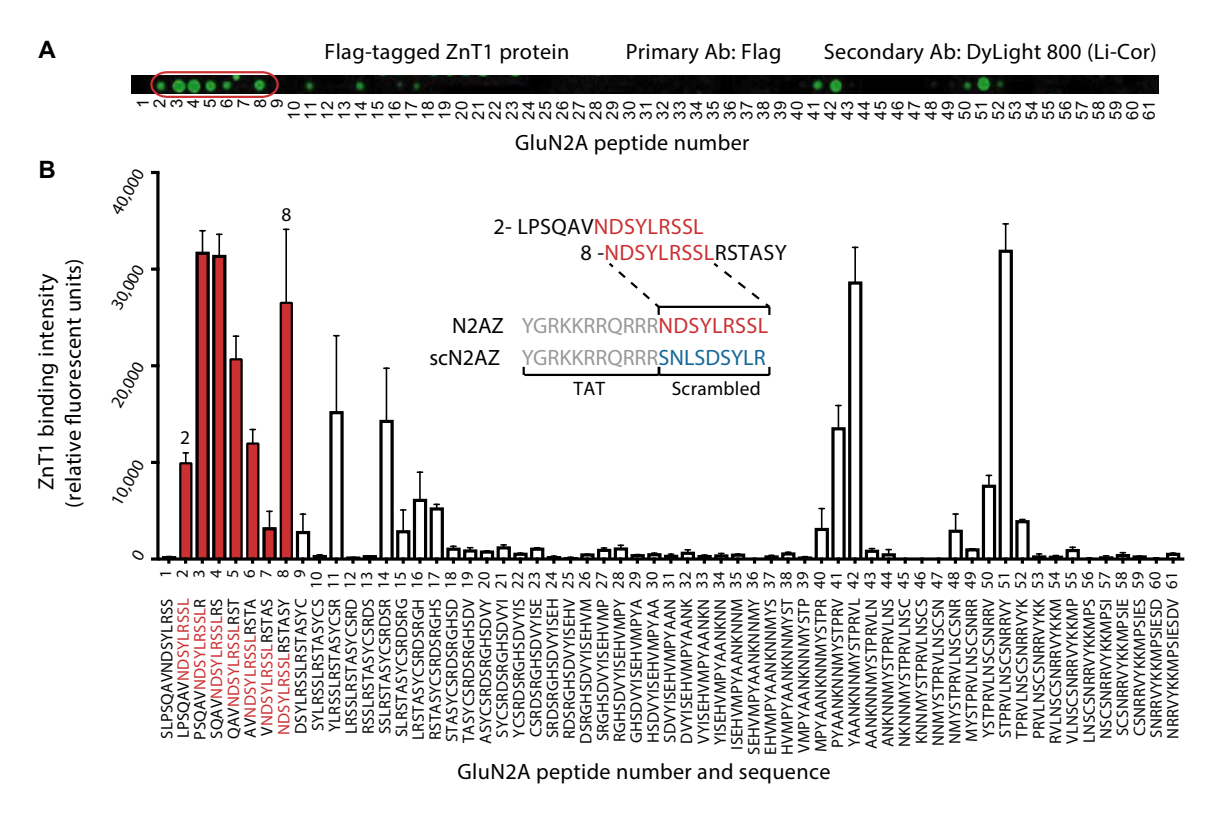


Fig. 1. Generation of a ZnT1-binding peptide (N2AZ) derived from the GluN2A C-terminal domain. (A) Peptide spot array was composed of sixty-one 15-mers spanning the GluN2A C-terminal region (residues 1390 to 1464) with 14-amino acid overlapping sequential sequences used to identify regions of high ZnT1 binding. A representative array is shown, with corresponding peptide numbers denoted below the blot. Sequences for each peptide number are shown in (B). The peptides denoting the broadest ZnT1-binding region are outlined in red. (B) Mean ± SEM (n = 4) of ZnT1-binding intensity for each GluN2A-derived peptide. Inset: Peptide sequences flanking a region of high ZnT1 binding (peptide numbers 2 to 8, in red) were used to determine the shared peptide sequence of the ZnT1-binding peptides. Sequence in light gray represents the cell-permeable HIV TAT domain sequence. The red sequence represents the final peptide, and the blue sequence represents its scrambled control. Both peptides were conjugated to TAT to create our experimental (N2AZ) and control (scN2AZ) peptides.

inset) were conjugated to the trans-activator of transcription (TAT) cell-penetrating peptide (YGRKKRRQRRR) to endow them with membrane permeability. As it was designed to prevent ZnT1-GluN2A binding, the peptide and its scrambled control will here be referred to as N2AZ and scN2AZ, respectively.

To confirm that N2AZ prevents GluN2A-derived sequences from binding to ZnT1, the peptide spot assay was repeated in the presence of either N2AZ or scN2AZ (100  $\mu M$ ). We noted that N2AZ reduced ZnT1 binding to the spot array when compared to scN2AZ control (fig. S1). These results indicate that N2AZ can disrupt the ZnT1-GluN2A association.

In the next set of experiments, we used rat cortical cultures to determine whether N2AZ treatment was sufficient to disrupt ZnT1-GluN2A association in neurons. We first verified that ZnT1 mRNA was expressed in cortical cultures using quantitative polymerase chain reaction (PCR). ZnT1 mRNA expression increased over the first 4 weeks in culture (fig. S2), with maximal expression levels observed after 19 days in vitro (DIV). The developmental expression profile of ZnT1 parallels, to some extent, that of GluN2A expression in the same preparation, with this NMDA receptor subunit's mRNA becoming highly detectable after 15 DIV (26). To quantify ZnT1-GluN2A interactions in the cultures, we used a proximity ligation assay (PLA), a method that produces discrete fluorescent puncta when target proteins are within 40 nm of one another, thus revealing putative protein-

protein interactions (*27*). Cultures (20 to 27 DIV) were treated overnight with either scN2AZ or N2AZ (3  $\mu$ M) before performing PLA. To visualize neurons, cultures were also immunostained for neuron-specific microtubule-associated protein 2 (MAP2). We observed that PLA puncta localized along neuronal dendrites, consistent with previous findings localizing ZnT1 to postsynaptic density (Fig. 2A) (*22*, *23*). We found that N2AZ treatment reduced the number of PLA puncta when compared to sister cultures treated with scN2AZ (paired *t* test, P = 0.004; n = 4; Fig. 2B). These results indicate that N2AZ effectively disrupts ZnT1-GluN2A interactions in cultured neurons.

## Disrupting the ZnT1-GluN2A association reduces zinc inhibition of NMDAR currents in cortical neurons in vitro

Zinc is an allosteric inhibitor of NMDARs through high-affinity binding on the extracellular, N-terminal domain of the GluN2A subunit (4, 20). As ZnT1 shuttles neuronal intracellular zinc to the extracellular space (28), we hypothesized that ZnT1 functionally localizes zinc in close proximity to its GluN2A-binding site and thereby contributes to the inhibition of NMDARs by the metal. To test this hypothesis, we treated DIV 20 to 27 cortical cultures overnight with either N2AZ or scN2AZ (3  $\mu$ M) before recording NMDAR-mediated currents. These currents were evoked by photolytic uncaging of 4-methoxy-7-nitroindolinyl (MNI)–caged glutamate (40  $\mu$ M) along the dendrites of neurons (Fig. 3A). Neurons were held at -70 mV

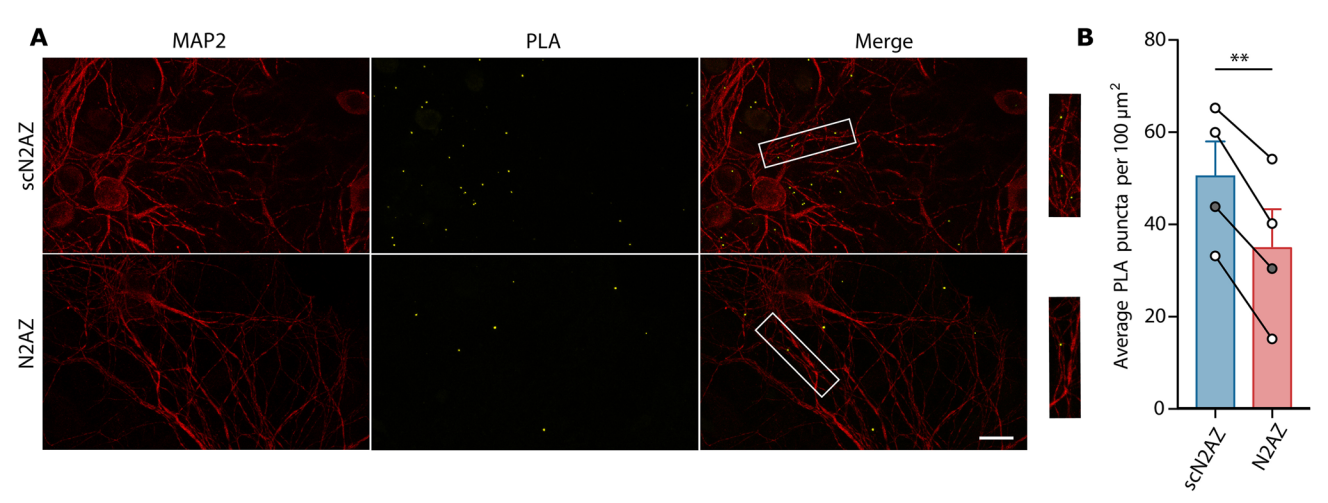


**Fig. 2. N2AZ disrupts ZnT1-GluN2A association.** (**A**) Representative images of rat cortical cultures following PLA between GluN2A and ZnT1. The PLA immunofluorescently labeled sites of interaction between GluN2A and ZnT1 (white puncta). In addition, MAP2 is immunofluorescently labeled in red to visualize neuron morphology. Scale bar,  $50 \, \mu m$ . Top row shows PLA following overnight exposure to  $3 \, \mu M$  scN2AZ, while bottom row shows PLA following 3  $\mu M$  N2AZ treatment. Insets show the localization of PLA puncta along a MAP2-stained dendrite. (**B**) Quantification of PLA puncta per  $100 \, \mu m^2$  in sister cortical cultures treated overnight with  $3 \, \mu M$  N2AZ or scN2AZ shows that N2AZ significantly reduced the number of ZnT1-GluN2A interactions compared to scN2AZ (paired t test, P = 0.0044; n = 4). Gray-filled circles indicate the quantification of representative images in (A). Error bars indicate mean  $\pm$  SEM.

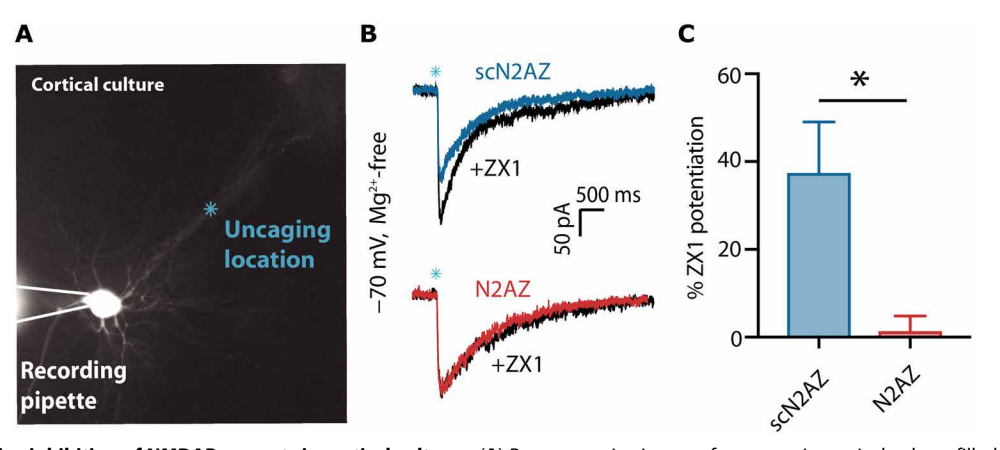


**Fig. 3. N2AZ reduces zinc inhibition of NMDAR currents in cortical cultures.** (**A**) Representative image of a neuron in cortical culture filled with Alexa 548 during whole-cell recording. Blue asterisk represents one example location of laser photolysis of MNI-caged glutamate (40 μM, 1-ms pulse) used to evoke EPSCs. (**B**) Sample traces of NMDAR currents, averaged over four sweeps, evoked by photolysis of MNI-caged glutamate in cultured cortical neurons held at -70 mV in Mg2<sup>+</sup>-free solution, before (blue, scN2AZ; red, N2AZ; 3 μM, treated overnight) and after application of ZX1 (black; 100 μM). (**C**) ZX1 potentiation of NMDAR currents was significantly diminished in N2AZ-treated cells versus scN2AZ control (unpaired t test, P = 0.01; n = 10, 9). Bar graphs represent the average potentiation of responses 5 min after ZX1 application. Error bars indicate mean  $\pm$  SEM. \*P < 0.05.

in the absence of extracellular  ${\rm Mg}^{2^+}$  to prevent block of NMDARs by this cation and in the presence of DNQX (20  $\mu$ M) to block AMPA receptor (AMPAR) currents. Zinc inhibition was determined by measuring the extent of NMDAR excitatory postsynaptic current (EPSC) potentiation following application of ZX1 (3  $\mu$ M), a fast, high-affinity, zinc-specific, extracellular chelator (3, 4, 9). We observed that extracellular zinc chelation with ZX1 produced a potentiation of NMDAR-mediated currents in scN2AZ-treated neurons (37.40  $\pm$  11.63% potentiation; n = 10; P = 0.02, paired t test of peak responses before and after ZX1), likely reflective of a background tonic zinc inhibition (Fig. 3, B and C). In contrast, N2AZ-treated neurons did not show any ZX1 potentiation of NMDAR-mediated currents (1.34  $\pm$  3.48%, n = 9, P = 0.62, paired t test; scN2AZ versus N2AZ, P = 0.01, unpaired t test; Fig. 3, B and C). Together, these

results indicate that ZnT1-GluN2A binding is critical for endogenous zinc inhibition of NMDAR-mediated currents in cortical neuronal cultures.

#### N2AZ reduces zinc inhibition in DCN synapses

To investigate whether ZnT1 contributes to synaptic zinc inhibition of NMDARs, we performed electrophysiological recordings in acutely prepared brain slices of the DCN, an auditory brainstem nucleus containing parallel fibers with zinc-rich synaptic terminals (29). In response to parallel fiber stimulation, synaptic zinc inhibits both NMDA and AMPA-mediated synaptic currents in cartwheel cells (3, 4), interneurons in the molecular layer of the DCN. In these synapses, at 20-Hz synaptic stimulation frequency, zinc chelation with ZX1 does not potentiate NMDARs in ZnT3 null [knockout (KO)] mice,

supporting the idea that ZnT3-dependent, extracellular, synaptically released zinc is necessary for zinc inhibition of NMDARs (4).

Here, we stimulated parallel fibers at 20 Hz and isolated NMDAR EPSCs by voltage-clamping cartwheel cells at +40 mV to relieve the Mg<sup>2+</sup> block while recording in the presence of DNQX (20  $\mu$ M). Slices were incubated with either scN2AZ or N2AZ (3  $\mu$ M) for at least 1 hour before ZX1 application (100  $\mu$ M). We found that N2AZ significantly reduced the ZX1 potentiation of NMDAR EPSCs when compared to scN2AZ (N2AZ: 19.39  $\pm$  5.82%, n = 14 versus scN2AZ: 47.30  $\pm$  10.14%, n = 9; unpaired t test, P = 0.02; Fig. 4, A to C). This result indicates that, contrary to the decades-long current model, synaptically released zinc alone is necessary but not sufficient to account for complete inhibition of NMDAR by the metal. Instead, these results show that synaptic zinc inhibition of NMDARs also requires the association of ZnT1 with GluN2A.

Knowing that synaptic zinc inhibition of NMDARs is abolished in ZnT3 KO mice (4), we next tested the actions of N2AZ in wild-type (WT) and ZnT3 KO mice. We found that ZX1 had no significant effects on NMDAR EPSCs in either KO or WT N2AZ-treated slices (KO:  $11.9 \pm 6.90\%$  potentiation, n=6, one-sample t test, P=0.13; WT:  $5.60 \pm 4.38\%$  potentiation, n=8, one-sample t test, P=0.27; fig. S3). This finding indicates that in the absence of the association of ZnT1 with GluN2A, the presence of vesicular zinc is of no consequence to zinc inhibition of NMDARs in either WT or ZnT3 KO mice, further supporting our main hypothesis on the crucial role of GluN2A-ZnT1 association on zinc inhibition of NMDARs.

We previously reported that at high-frequency trains of synaptic stimulation (100 to 150 Hz), ZX1 potentiates NMDAR EPSCs in WT mice to the same extent as in ZnT3 KO mice, indicating that an additional, ZnT3-independent source of zinc, referred to as tonic (4), also inhibits NMDAR EPSCs. As such, we next evaluated the contribution of the ZnT1-GluN2A interaction in response to high-frequency stimulation synaptic stimulation. At 100-Hz stimulation frequency, we found that N2AZ treatment eliminated ZX1 potentiation of NMDAR EPSCs, suggesting that ZnT1-GluN2A interaction is also required for tonic, ZnT3-independent zinc inhibition (1.95  $\pm$  4.33%; n = 14; P = 0.45, paired t test of responses before and after ZX1; Fig. 4, D to F ). Together, our results indicate that ZnT1-GluN2A binding is critical for both ZnT3-dependent and ZnT3-independent inhibition of NMDARs.

#### N2AZ effects are limited to the ZnT1-GluN2A association

In addition to blocking NMDAR EPSCs, synaptically released zinc inhibits AMPAR EPSCs in cartwheel cells (3). To test whether the aforementioned actions of N2AZ are specific for NMDAR EPSCs, we measured the effect of N2AZ and scN2AZ on zinc inhibition of AMPAR EPSCs. We observed that ZX1 potentiated AMPAR EPSCs to a similar extent regardless of the treatment with either scN2AZ or N2AZ (scN2AZ: 30.3  $\pm$  10.24%, n = 6; N2AZ: 29.3  $\pm$  6.70, n = 6; unpaired t test, P = 0.93; Fig. 5, A and B), indicating that N2AZ reduces zinc inhibition of NMDAR EPSCs without affecting AMPAR EPSCs.

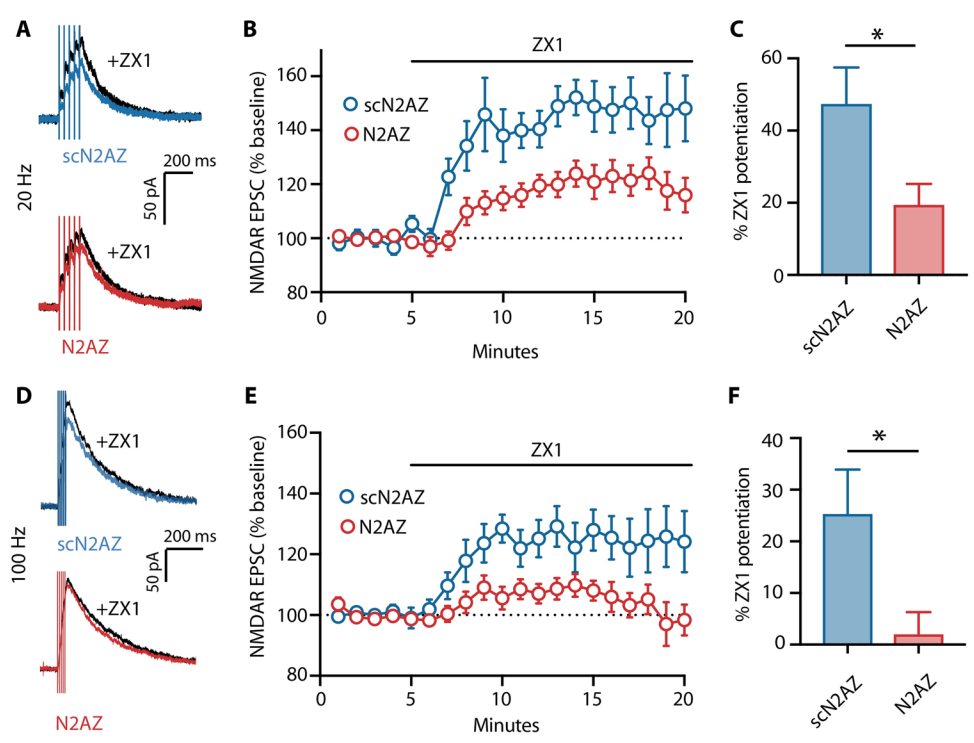
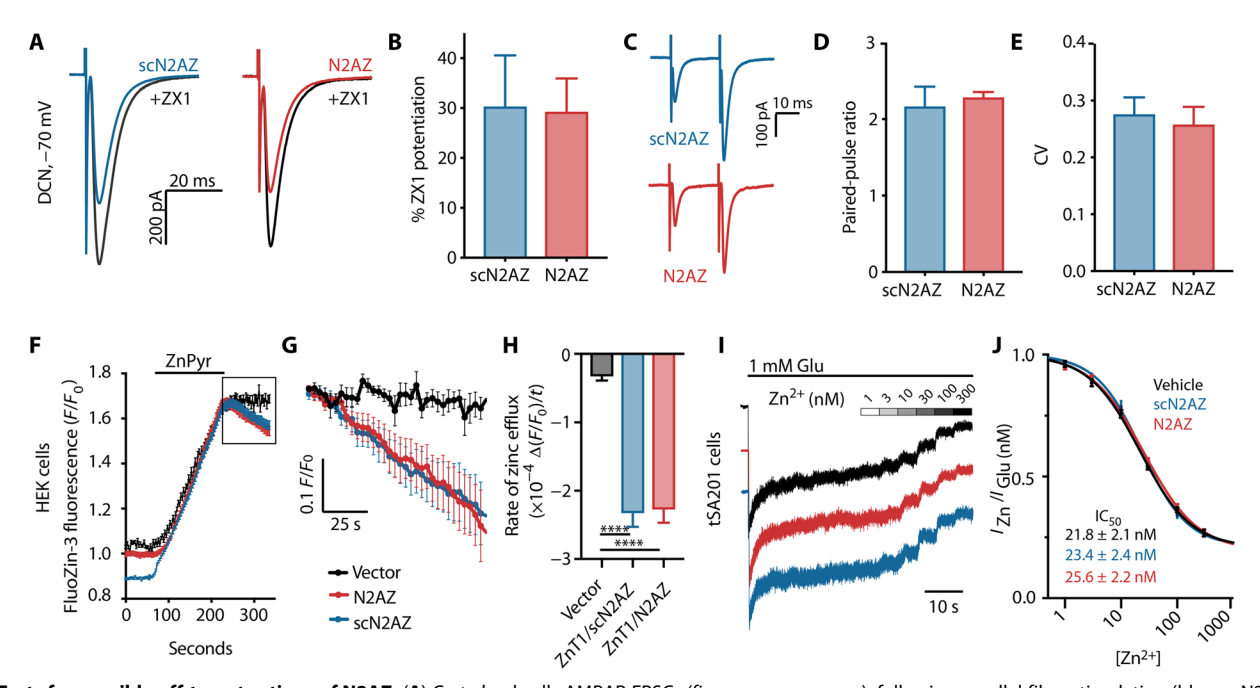


Fig. 4. N2AZ reduces ZnT3-dependent and ZnT3-independent inhibition of NMDAR EPSCs in DCN cartwheel cells. (A and D) Sample traces of NMDAR EPSCs, averaged over five sweeps, evoked in cartwheel cells in response to five pulses at 20-Hz (A) or 100-Hz (D) stimulation frequency of parallel fibers. Before (blue, scN2AZ; red, N2AZ;  $3 \mu M$ , treated  $\geq 1$  hour before recording) and after application of ZX1 (black;  $100 \mu M$ ). (B and E) Time course of NMDAR EPSCs, normalized to a 5-min baseline before addition of ZX1. Dotted line marks 100% of baseline. (C and F) Group data show that ZX1 potentiation of EPSCs was significantly reduced in N2AZ- versus scN2AZ-treated slices for 20-Hz stimulation (unpaired t test, P = 0.02; n = 14, 9) and 100-Hz stimulation (unpaired t test, P = 0.02; n = 14, 9). Bar graphs represent the average potentiation of responses 10 to 15 min after 2X1 application. Error bars indicate mean  $\pm \text{ SEM}$ . \*P < 0.05.



**Fig. 5. Tests for possible off-target actions of N2AZ.** (**A**) Cartwheel cells AMPAR EPSCs (five sweep averages), following parallel fiber stimulation (blue, scN2AZ; red, N2AZ; 3 μM throughout this figure) in the absence and presence of ZX1 (black;  $100 \mu M$ ). (**B**) ZX1 potentiation of AMPAR EPSCs (n = 3) is not different between treatments. (**C**) Sample traces of AMPAR EPSCs (50-ms interstimulus interval). (**D** and **E**) Average paired-pulse ratio (D) and coefficient of variance (CV; E) are not different between treatments (mean ± SEM; n = 3). (**F**) FluoZin-3 fluorescence in HEK293 cells transfected with vector (black), ZnT1 with scN2AZ treatment (blue), or ZnT1 with N2AZ treatment (red). Zinc (1 μM, with 5 μM pyrithione) treatment increases intracellular zinc (black bar). Zinc efflux was measured (box) as decreases in fluorescence. (**G**) Average showing the change in fluorescence after zinc washout. (**H**) Zinc efflux rates as the slope of the average fluorescence traces in (G). ZnT1-transfected cells exhibited greater zinc efflux compared to vector-transfected controls (one-way ANOVA/Tukey N2AZ versus vector, scN2AZ versus vector; P < 0.0001, n = 4 to 5); scN2AZ and N2AZ treatments do not differ. (I) Glutamate (1 mM, black bar)–evoked currents in GluN1/2A-transfected HEK-tsa201 cells (-60 mV; Mg<sup>2+</sup>-free) with increasing concentrations of zinc (1 to 300 nM). (J) Zinc inhibition curves; insets = IC<sub>505</sub> (mean ± SEM; n = 5), vehicle-treated (black), scN2AZ-treated (3 blue), and N2AZ-treated (red) cells; all are similar (P = 0.5).

We also evaluated whether a change in presynaptic release of glutamate contributes to the observed actions of N2AZ on NMDARmediated synaptic currents. We used two independent measures of release probability: paired-pulse ratio (PPR) and the coefficient of variance (CV). Both measures vary inversely with probability of release. For PPR measurements, we applied two stimuli in rapid succession (50-ms interstimulus interval) to compute the amplitude ratio of the second to the first EPSC. We calculated CV as the SD of a series of EPSCs divided by their mean amplitude. We found that scN2AZ and N2AZ altered neither PPR nor CV (PPR: scN2AZ: 2.18 ± 0.26, n = 3; N2AZ: 2.29  $\pm$  0.07, n = 5, unpaired t test, P = 0.59; CV:  $scN2AZ: 0.28 \pm 0.030, n = 3; N2AZ: 0.26 \pm 0.031, n = 5, unpaired t test,$ P = 0.76; Fig. 5, C to E). As such, N2AZ's effects on zinc inhibition of NMDAR-mediated synaptic currents are not associated with changes in presynaptic glutamate release probability. These observations also rule out potential actions of N2AZ either on zinc signaling via the metabotropic zinc receptor GPR39 or on NMDAR-dependent, metabotropic activation of pannexin-1, as both signaling mechanisms are associated with changes in presynaptic glutamate release probability (11, 30).

To control for potential effects of N2AZ on the ZnT1 transporter activity, we next examined whether N2AZ modifies transport itself. Following intracellular zinc loading, we measured decreases in intracellular zinc levels over time as a readout of zinc transport in HEK293 cells previously transfected with a plasmid encoding ZnT1 or with an empty vector. We used FluoZin-3 fluorescence to measure intracellular zinc levels. FluoZin-3–loaded cells were briefly treated

with zinc pyrithione (1  $\mu$ M Zn<sup>2+</sup> and 5  $\mu$ M sodium pyrithione) to increase intracellular zinc concentrations until the fluorescent signal reached a maximum, steady-state level (Fig. 5F). Zinc efflux was then measured as the decrease in FluoZin-3 fluorescence (Fig. 5G). As expected, ZnT1-expressing cells showed significantly more zinc efflux than vector-transfected controls [one-way analysis of variance (ANOVA),  $P \le 0.0001$ ; Tukey multiple comparisons, N2AZ versus vector, scN2AZ versus vector,  $P \le 0.0001$ ; Fig. 5H]. However, the rate of zinc efflux was not different in ZnT1-expressing cells treated with either scN2AZ or N2AZ [-0.0002273 ( $F/F_0$ )/s, n = 5] or scN2AZ [-0.0002327 ( $F/F_0$ )/s, n = 4] (Tukey multiple comparisons, N2AZ versus scN2AZ, P = 0.97), indicating that N2AZ's actions on zinc inhibition of NMDARs cannot be explained by alterations in ZnT1 zinc transport activity.

To control for potential effects of N2AZ on NMDAR affinity for zinc itself, we measured NMDAR inhibition by exogenous zinc application onto HEK cells previously transfected with plasmids encoding GluN1 and GluN2A. Exogenous, extracellular zinc was applied across a wide range of concentrations (1 to 300  $\mu$ M) using a multi-barreled rapid-perfusion system while recording glutamate (1 mM)-evoked steady-state GluN1/2A receptor current. The calculated IC<sub>50</sub>s (median inhibitory concentrations) for zinc block in vehicle, scN2AZ-treated, or N2AZ-treated cells were not different across the three treatments, indicating that N2AZ does not affect zinc's affinity for GluN1/2A receptors (IC<sub>50</sub> in nM; vehicle: 21.8  $\pm$  2.1, n = 5; scN2AZ: 23.4  $\pm$  2.4, n = 5; N2AZ = 25.6  $\pm$  2.2, n = 5; ordinary one-way ANOVA, P = 0.4996). Taking all of these results

together, we conclude that N2AZ reduces zinc inhibition of NMDARs by disrupting the ZnT1-GluN2A interaction, without affecting glutamate release, ZnT1-dependent zinc transport, or zinc affinity for GluN1/2A receptors. Moreover, these results suggest that N2AZ does not have either toxic or nonspecific effects.

### Postsynaptic intracellular zinc is necessary for synaptic zinc inhibition of NMDARs

The simplest model to explain our results thus far is that the ZnT1-GluN2A interaction is necessary for zinc inhibition of NMDARs by transporting zinc from the cytoplasm of the postsynaptic cell to the extracellular space and in close proximity to the NMDAR. This model predicts that postsynaptic intracellular zinc is therefore also necessary for zinc inhibition of NMDARs. Because ZX1 is cell impermeant, we opted to selectively chelate intracellular zinc by including ZX1 (100  $\mu M$ ) in the recording pipette, allowing us to test the contribution of intracellular zinc to synaptic zinc inhibition of NMDARs. ZX1 in the recording pipette was allowed to diffuse into the patched cell for at least 30 min before applying extracellular ZX1. We observed that intracellular ZX1, applied via the recording pipette, blocked extracellular ZX1 potentiation of NMDAR EPSCs

 $(5.23 \pm 4.22\%; n = 6; P = 0.64, paired t test of responses before and$ after ZX1; Fig. 6, A and B). In contrast, control experiments, without ZX1 in the recording pipette and assessed 30 min before applying extracellular ZX1, showed robust potentiation of NMDAR EPSCs (Fig. 6, A and B:  $32.10 \pm 6.36\%$ ; n = 6; P = 0.009, paired t test of responses before and after ZX1; Fig. 6C: intracellular ZX1 versus control; P = 0.006, unpaired t test). This result indicates that intracellular postsynaptic zinc is required for synaptic zinc inhibition of NMDARs. Together, these results show that this intracellularly originated zinc pool along with the ZnT3-dependent extracellular zinc are both necessary for zinc inhibition of NMDAR EPSCs. As current models have been suggesting that zinc inhibition of synaptic NMDARs depends exclusively on presynaptically released extracellular zinc, this is an important finding that changes this dogma and significantly advances our understanding of a fundamental synaptic mechanism of neuromodulation.

We next examined whether the well-established routes of entry for zinc into neurons, including calcium-permeable AMPAR (31) and L-type calcium channels (32), mediate potential translocation of synaptic zinc into the cytoplasm of cartwheel cells. AMPARs were immediately ruled out by the fact that all our experiments were performed in the

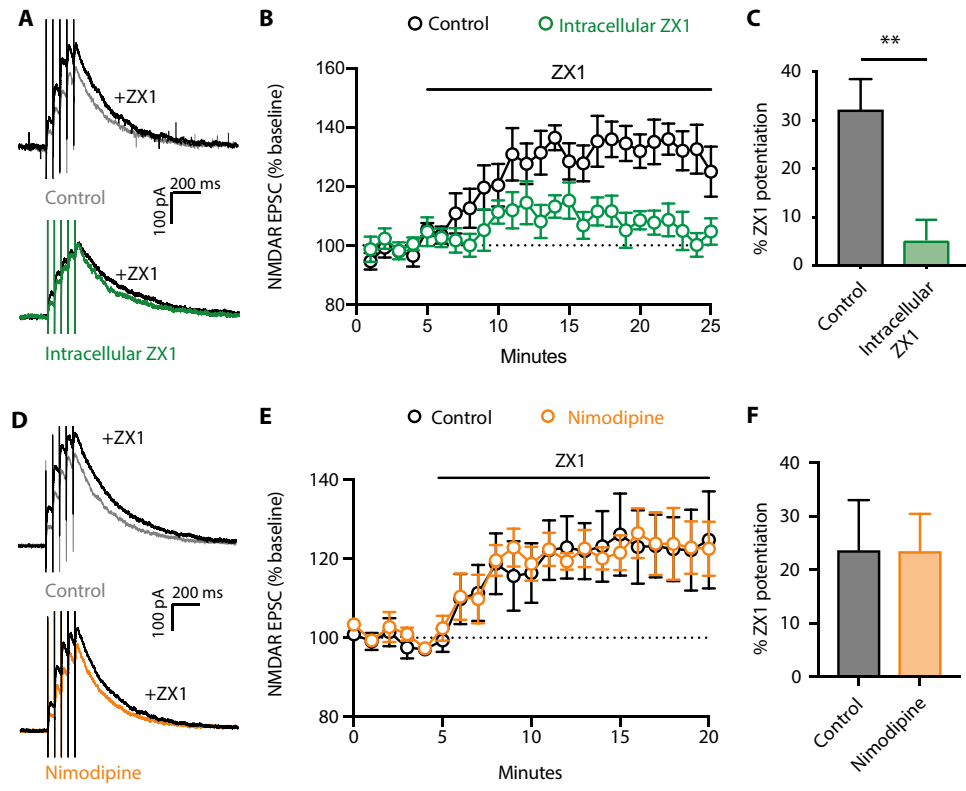


**Fig. 6. Chelating intracellular zinc reduces zinc inhibition of NMDAR EPSCs. (A)** Sample NMDAR EPSCs at +40 mV, average of five sweeps, in response to five pulses at 20-Hz stimulation frequency, before and after application of extracellular ZX1 (100 μM) in control (no intracellular ZX1) and in 100 μM intracellular ZX1. (**B**) Time course of NMDAR EPSCs normalized to a 5-min baseline in control (black) and intracellular ZX1 (green) showing the effect of ZX1 on NMDAR EPSCs. Dotted line marks 100% of baseline. (**C**) Group data show that intracellular ZX1 significantly reduced extracellular ZX1 potentiation of NMDAR EPSCs compared to control [unpaired *t*-test, P = 0.006, n = 6 (control), 8 (intracellular ZX1)]. Bar graphs represent the average potentiation of responses 15 to 20 min after ZX1 application. \*\*P < 0.01. (**D**) Sample traces of NMDAR EPSCs at +40 mV, average of five sweeps, in response to five pulses at 20-Hz stimulation frequency, before and after application of extracellular ZX1 (100 μM) in control (0.01% DMSO) and nimodipine (20 μM nimodipine in 0.01% DMSO), ≥20 min before beginning of recordings. (**E**) Time course of NMDAR EPSCs normalized to 5-min baseline in control (black) and extracellular nimodipine (orange) before and after ZX1 application (black bar, above). Dotted line marks 100% of baseline. (**F**) Group data show that ZX1 potentiation was not significantly different between nimodipine and control [unpaired *t* test, P = 0.99; n = 6 (control), 4 (nimodipine)]. Bar graphs represent the average potentiation of responses 10 to 15 min after ZX1 application. Error bars indicate mean ± SEM.

presence of DNQX. As previous reports have shown that L-type calcium channels can also interact with ZnT1 (33), we examined whether these channels contribute to synaptic zinc inhibition of NMDARs. We applied nimodipine (20  $\mu$ M) for at least 20 min before recordings to inhibit L-type calcium channels and measured zinc inhibition of NMDAR responses. We observed no significant differences in ZX1 potentiation of NMDAR EPSCs between nimodipine-treated slices (23.6  $\pm$  6.9%, n = 4; Fig. 6, D to F) and vehicle-treated [dimethyl sulfoxide (DMSO)] slices (23.6  $\pm$  9.4%; n = 6; unpaired t test, P = 0.997), indicating that the putative translocation of synaptic zinc to postsynaptic neurons via L-type calcium channels does not contribute to zinc inhibition of NMDARs.

#### DISCUSSION

Current models suggest that zinc inhibition of synaptic NMDARs depends exclusively on presynaptically released zinc. In contrast, our results indicate that zinc inhibition of NMDAR EPSCs also requires postsynaptic zinc and the presence of GluN2A-ZnT1 association. Our results demonstrate that the physical dissociation of GluN2A and ZnT1 by the newly developed peptide N2AZ diminished the inhibitory actions of synaptic zinc on NMDAR EPSCs. Moreover, chelation of postsynaptic intracellular zinc abolished zinc inhibition of NMDARs. Before the work presented here, it had been generally assumed that zinc cleft concentrations following its synaptic release were sufficient to directly inhibit NMDAR function (1, 2, 4, 9, 16), without involvement of the transport pathway uncovered by our work. However, here, we show that ZnT1-GluN2A association is also necessary for zinc to be rapidly localized to physiologically relevant microdomains in very close proximity to the GluN2Acontaining NMDARs. This is highly reminiscent of calcium microdomains that have been postulated for a number of synaptic functions, including rapid synaptic release of neurotransmitters (34). Whether similar transport processes are in place for synaptic zinc to activate or modify other known postsynaptic targets for the metal, including the metabotropic zinc receptor GPR39 (19) or AMPAR-mediated synaptic currents (3), remains to be determined.

Why the DCN synapses need both extracellular and intracellular zinc for synaptic zinc inhibition of NMDARs? This may be the result of the complex nature of zinc as a signaling molecule itself (9, 35). As alluded to earlier, zinc is a promiscuous ligand that acts on a variety of postsynaptic targets (3, 6, 11, 18, 36). Moreover, not all vesicles at zinc-rich synaptic terminals contain zinc (37, 38), and zinc-containing vesicle release probability can change with varying levels of activity (37, 39). Therefore, maintaining adequate signaling requires precise spatial zinc regulation, in addition to presynaptic release. The ZnT1-GluN2A interaction may be reflective of a system that harnesses and directs zinc's signaling properties while supplying and maintaining specificity of action for a given activity level. As NMDAR function is regulated by subunit composition (40), as well as by its localization in postsynaptic structures (41), ZnT1 may endow the zinc-containing synapse with a dynamic form of regulation specific for GluN2A-containing NMDAR signals.

ZnT1 expression is also tightly coupled to fluctuations in free intracellular zinc levels (42). Rises in intracellular zinc concentrations are quickly detected by the metal regulatory element (MRE) transcription factor 1 (MTF1) to induce up-regulation of MRE-driven genes, including ZnT1 (43). As increases in intracellular zinc levels have been prominently detected following neuronal depolarization

(44), it is also conceivable that the ZnT1-GluN2A complex is a key component of activity-dependent synaptic processes, perhaps even in synapses that do not express ZnT3, and, thereby, vesicular zinc. Robust NMDAR activation can lead to intracellular zinc liberation from metal-binding proteins such as metallothionein (45), independently of synaptic zinc (46), likely as a consequence of glutamate-stimulated production of oxygen-derived reactive species (47). We suggest that the observed actions of N2AZ on ZnT3-independent zinc inhibition of NMDAR-mediated responses (i.e., caged glutamate responses in cortical neurons in culture and 100-Hz stimulation of parallel fibers; Figs. 3 and 4, E to G) may be reflective of increases of intracellular zinc in response to robust NMDAR activation produced under our experimental conditions. Manipulations that enhance or diminish ZnT1 expression in cultured neurons have yielded subsequent increases or decreases in dendritic spine length, respectively (23). As NMDAR activation is a major regulator of synaptic strength and spine dynamics, ZnT1-mediated zinc inhibition may provide unique forms of synaptic plasticity through its regulation of NMDAR function.

One remaining question not fully addressed in our study is how presynaptic release of zinc and postsynaptic transport of intracellular zinc by ZnT1 cooperate to regulate NMDARs. It is tempting to assume that the source of the postsynaptic intracellular pool of zinc necessary for NMDAR block is derived from the synaptically released pool, translocating to the postsynaptic neuron. However, the predominant routes of entry for zinc (L-type calcium channels and AMPARs do not appear to contribute to zinc inhibition of NMDAR inhibition. SLC39A (Zrt- and Irt-like Proteins; ZIP) transporters, which move zinc into the cytoplasm, may serve as the route for synaptic zinc translocation, and both ZIP1 and ZIP3 have been previously observed to influence synaptic uptake of zinc, albeit under injurious conditions (48). However, further experiments will be necessary to fully assess the complex interplay between ZnT3 and ZnT1 to regulate zinc inhibition of NMDARs.

In summary, we developed a cell-permeant peptide that dissociates the zinc transporter ZnT1 from the highly zinc-sensitive NMDAR subunit GluN2A. This novel tool allowed us to uncover the mechanism by which zinc inhibits NMDAR function, which involves not only extracellular ZnT3-dependent zinc but also intracellular zinc and ZnT1-GluN2A complexes. We propose that the ZnT1-GluN2A association allows the synapse to direct zinc to its high-affinity binding site within the GluN2A-containing NMDAR by creating a physiologically and spatially distinct extracellular zinc microdomain in the synapse.

#### **MATERIALS AND METHODS**

#### **Experimental design and materials**

All animal procedures used in experiments were approved by the Institutional Animal Care and Use Committee of the University of Pittsburgh School of Medicine. Experiments in DCN slices were performed blind to the treatment. Experiments using ZnT3 KO and WT animals were performed blind to the genotype of the animal. All key materials used are summarized in the Supplementary Materials (table S1).

#### Neuronal cultures

Cortical cultures were prepared from embryonic day 16 rats. Briefly, pregnant rats (Charles River Laboratories) were sacrificed via CO<sub>2</sub> inhalation. Embryonic cortices were dissociated with trypsin and plated at 670,000 cells per well on 12-mm glass coverslips in six-well

plates. Non-neuronal cell proliferation was inhibited after 2 weeks in culture with cytosine arabinoside (1 to 2  $\mu$ M). Cultures were used during the 3 and 4 weeks in vitro (20 to 27 DIV) for PLA and electrophysiology experiments.

#### Cell line culture and transfection

HEK (HEK-tsa201) cells were maintained in Dulbecco's modified Eagle's medium (DMEM) supplemented with 10% fetal bovine serum and 1% GlutaMAX. Cells were plated in 35-mm petri dishes with three 15-mm glass coverslips treated with poly-D-lysine (0.1 mg/ml) and rat tail collagen (0.1 mg/ml) at a density of  $1 \times 10^5$  cells per dish. Eighteen to 30 hours after plating, the cells were cotransfected using FuGENE 6 Transfection Reagent with complementary DNA (cDNA) coding for enhanced green fluorescent protein (eGFP) for identification of transfected cells and the WT rat NMDAR subunits GluN1-1a (GluN1; GenBank X63255) and GluN2A (GenBank M91561 in pcDNA1). GluN1-1a and eGFP were expressed using a specialized pCl-neo vector with cDNA encoding eGFP inserted between the cytomegalovirus (CMV) promoter and the GluN1 open reading frame to express eGFP and GluN1 as separate proteins. At the time of transfection, 200 µM DL-2-amino-5-phosphonovaleric acid (APV) was added to culture medium to prevent NMDAR-mediated cell death. For experiments testing the effect of N2AZ and scN2AZ, cells were incubated with 3 µM peptide for 3 to 6 hours before recording.

#### **Proximity ligation assay**

PLAs were performed using a Duolink PLA kit. Cortical cultures were treated overnight with either N2AZ or scN2AZ (3 µM, dissolved in water). Coverslips were fixed in ice-cold methanol for 5 min, rinsed in phosphate-buffered saline (PBS), and then permeabilized with 0.1% Triton X in PBS. Coverslips were then incubated with primary antibodies: rabbit anti-ZnT1, mouse anti-GluN2A, and chicken anti-MAP2. Coverslips were incubated with a donkey anti-chicken fluorescent secondary antibody targeting MAP2 antibodies to visualize neuron morphology. The PLA reaction was then completed according to Duolink PLA protocol. Briefly, coverslips were incubated in Duolink secondary antibodies (anti-rabbit and anti-mouse), which are conjugated with complementary oligonucleotides. Ligation solution was added to hybridize connector oligonucleotides and PLA probes, allowing the oligonucleotides to join in a closed loop when secondary antibodies were in close proximity. Next, the reaction was amplified with rolling-circle amplification (RCA) using the closed loop hybridized probes as a template. PLA probes were fluorescently labeled with oligonucleotides, which hybridized to the RCA product during amplification. Coverslips from sister cultures were treated with either scN2AZ or N2AZ, and reactions were run simultaneously using the same preparation of reagents. Coverslips were mounted on glass slides using Duolink mounting medium, and four random fields of view were imaged from each coverslip using a 60× oil objective on a Nikon A1R laser scanning confocal microscope. PLA puncta, reflecting GluN2A-ZnT1 interactions, were counted automatically with Fiji ImageJ (version 2.0) software. We used maximum intensity projection of eight sequential images in the z plane. All images were normalized to the same intensity threshold using the Yen threshold setting before automated quantification of puncta.

PLA experiments were performed four independent times, each time from a different tissue culture (different pregnant dam). The n in Fig. 2 refers to the number of coverslips analyzed per treatment (scN2AZ versus N2AZ). The average and SEM of these experiments are shown in the bar graphs of Fig. 2. Each individual data point

shown in the same figure panel represents a single coverslip, each with an average of four images obtained in random areas within each coverslip.

For a given culture, cortical tissue is normally obtained from approximately eight rat brain embryos, pooled and dissociated; cultures are plated at a density of 680,000 cells per 35-mm culture dish. To plate the cells, we previously place five 12-mm coverslips in each 35-mm dish, although the area of the dish could accommodate six coverslips (that is, six coverslips would occupy nearly the entire area of the dish). This culture procedure results in approximately 20% neurons and 80% glia, mostly astrocytes (49). Thus, our best estimate is that, at most, there are ~22,500 neurons per coverslip (680,000  $\times$  0.2/6). We transfer individual coverslips from this culture dish to a separate culture plate to perform each experiment noted.

#### **Brain slices**

Male and female mice (postpartum days 18 to 28) were anesthetized with isoflurane and sacrificed. Brains were rapidly dissected and sectioned with a vibratome (Leica, VT1000S) into 210- $\mu$ m-thick coronal slices of the brainstem containing DCN. Slices were incubated in artificial cerebrospinal fluid (ACSF) containing 130 mM NaCl, 3 mM KCl, 2.4 mM CaCl<sub>2</sub>, 1.3 mM MgCl<sub>2</sub>, 20 mM NaHCO<sub>3</sub>, 3 mM Hepes, and 10 mM glucose, saturated with 95% O<sub>2</sub>/5% CO<sub>2</sub> (v/v), pH ~7.3, ~300 mOsm at 35°C for 1 hour before being moved to room temperature. During preparation, ACSF was treated with Chelex 100 resin to remove any contaminating zinc. After applying Chelex to the ACSF, high-purity calcium and magnesium salts were added (99.995% purity). All plastic and glassware were washed with 5% high-purity nitric acid.

#### Electrophysiology

Whole-cell voltage-clamp recordings from HEK-tsa201 cells were performed 18 to 30 hours after transfection. Pipettes were fabricated from borosilicate capillary tubing (outside diameter, 1.5 mm; inside diameter, 0.86) using a Flaming Brown P-97 electrode puller (Sutter Instruments) and fire-polished to a resistance of 2.5 to 4.5 megohms with an in-house fabricated microforge. Intracellular pipette solutions consisted of 130 mM CsCl, 10 mM Hepes, 10 mM 1,2-bis(2aminophenoxy)ethane-N,N,N',N'-tetraacetic acid (BAPTA), and 4 mM MgATP with pH balanced to 7.2 ± 0.05 using CsOH and final osmolality of 280 ± 10 mOsm. Extracellular recording solution contained 140 mM NaCl, 2.8 mM KCl, 1 mM CaCl<sub>2</sub>, 10 mM Hepes, 10 mM tricine, and 0.1 mM glycine and was balanced to pH 7.2 ± 0.05 and osmolality 290 ± 10 mOsm with NaOH and sucrose, respectively. Glutamate (Glu) and ZnCl<sub>2</sub> were diluted from concentrated stock solutions in extracellular solution each day of experiments. Buffered Zn<sup>2+</sup> solutions were prepared as previously described (20) via serial dilution. Extracellular solutions were delivered to the cell using a fast perfusion system. Whole-cell currents were recorded using an AxoPatch 200A patch-clamp amplifier (Molecular Devices), low pass-filtered at 5 kHz, and sampled at 20 kHz in pClamp10.7 (Molecular Devices). In all recordings from HEK-tsa201cells, series resistance was compensated 85 to 90% and an empirically determined -6-mV liquid junction potential between the intracellular pipette solution and the extracellular recording solution was corrected.

The effect of the N2AZ on  $\rm Zn^{2+}$  inhibition of GluN1/2A receptors was determined using the protocol shown in Fig. 5I. Glu (1 mM) was applied for 30 s until current reached steady state, followed by sequential applications (5 s each) of 1 mM Glu and  $\rm Zn^{2+}$  at 1, 3, 10, 30, 100, and 300 nM. A final 30-s application of Glu in the absence

of  $Zn^{2+}$  was then performed to allow recovery from inhibition.  $Zn^{2+}$  IC<sub>50</sub> was estimated by fitting the following equation to data

$$\frac{I_{\rm Zn}}{I_{\rm Glu}} = A + \frac{1 - A}{1 + \left(\frac{[{\rm Zn}^{2+}]}{{\rm IC}_{50}}\right)^{n_H}}$$

where  $I_{\rm Zn}/I_{\rm Glu}$  was calculated as the mean current over the final 1 s of  $\rm Zn^{2+}$  application divided by the average of the mean steady-state currents (final 1 s) elicited by Glu before and after  $\rm Zn^{2+}$  application. A  $(I_{\rm Zn}/I_{\rm Glu}$  at saturating  $\rm Zn^{2+}$ ), IC<sub>50</sub>, and  $n_{\rm H}$  (Hill coefficient) were free parameters during fitting. Curve fitting and statistical comparisons were performed in Prism 8. IC<sub>50</sub>s were compared by oneway ANOVA.

Whole-cell recordings from cultured cortical neurons were obtained with glass micropipettes (3 to 6 megohms) containing 140 mM CsF, 10 mM CsEGTA, 1 mM CaCl<sub>2</sub>, and 10 mM Hepes, pH 7.2, 295 mOsm. Extracellular recording solution contained 150 mM NaCl, 2.8 mM KCl, 1.0 mM CaCl<sub>2</sub>, 10 mM Hepes, and 10 μM glycine, pH ~7.2, ~300 mOsm. Using Ephus and a Multiclamp 700B amplifier (Molecular Devices), NMDAR EPSCs were recorded in voltage clamp (held at -70 mV) in the presence of tetrodotoxin (300 nM, sodium channel blocker), DNQX (20 µM, AMPA and kainate receptor antagonist), and MNI-caged glutamate (40 µM). Neurons were visualized by including 10 µM Alexa 594 in the internal solution. To evoke NMDAR EPSCs, we photolytically uncaged MNI-caged glutamate onto dendrites at four locations 0, 40, 80, and 120 µm from the cell soma using 1-ms pulses of ultraviolet laser light (355 nm, DPSS Lasers). The ZX1-mediated potentiation for each cell was calculated as the average percent increase in responses following application of the metal chelator across these four uncaging locations.

For brain slice recordings, whole-cell recordings of NMDAR EPSCs of DCN cartwheel cells were obtained with micropipettes (3 to 6 megohms) containing 128 mM Cs(CH<sub>3</sub>O<sub>3</sub>S), 4 mM MgCl<sub>2</sub>•6H<sub>2</sub>O, 4 mM Na<sub>2</sub>ATP, 10 mM Hepes, 0.3 mM tris-GTP (guanosine triphosphate), 10 mM tris-phosphocreatine, 1 mM CsEGTA, 1 mM QX-314, and 3 mM sodium ascorbate, pH ~7.2, 300 mOsm in chelexed ACSF with the following composition: 130 mM NaCl, 3 mM KCl, 2.4 mM CaCl<sub>2</sub>, 1.3 mM MgCl<sub>2</sub>, 20 mM NaHCO<sub>3</sub>, 3 mM Hepes, and 10 mM glucose, saturated with 95% O<sub>2</sub>/5% CO<sub>2</sub> (v/v), pH ~7.3, ~300 mOsm. Cartwheel cells were identified by the presence of complex spikes (50) in cell-attached configuration before break-in or in response to current injections in current-clamp mode immediately after break-in. NMDAR EPSCs were recorded in voltage-clamp mode at a holding potential of +40 mV in the presence of DNQX (20 μM), SR95531 (20  $\mu$ M, GABA<sub>A</sub>R antagonist), and strychnine (1  $\mu$ M, GlyR antagonist). ZX1 (100 μM) was included in the pipette in experiments where noted. Whole-cell recordings of AMPAR EPSCs were obtained with micropipettes containing 113 mM K-gluconate, 4.5 mM MgCl<sub>2</sub>•6H<sub>2</sub>O, 14 mM tris-phosphocreatine, 9 mM Hepes, 0.1 mM EGTA, 4 mM Na<sub>2</sub>ATP, 0.3 mM tris-GTP, and 10 mM sucrose, pH 7.3, 295 mOsm. AMPAR EPSCs were recorded in voltage-clamp mode at a holding potential of -70 mV in the presence of SR95531 (20 µM) and strychnine (1 μM). Both NMDAR and AMPAR EPSCs were evoked using an Isoflex stimulator (A.M.P.I., 0.1-ms pulses) stimulating parallel fibers with voltage pulses through a theta glass electrode. For paired-pulse experiments, interstimulus interval was 50 ms. Once a stable response

was established, ZX1 (100 μM) was added to the recording solution to measure the effect of zinc chelation on EPSCs. The series resistance was not compensated because the currents measured were relatively small; therefore, there was minimum voltage-clamp error. The cell parameters were monitored during the recording by delivering -5-mV voltage steps for 50 ms at each sweep. The peak current value ( $\Delta I_{\text{peak}}$ ) generated immediately after the step in the command potential was used to calculate series resistance ( $R_{\text{series}}$ ) using the following formula:  $R_{\text{series}} = -5 \text{ mV}/\Delta I_{\text{peak}}$ . The difference between baseline and steady-state current ( $\Delta I_{ss}$ ) was used to calculate input resistance ( $R_{\rm I}$ ) using the following formula:  $R_{\rm I} = -5 \text{ mV}/\Delta I - R_{\rm series}$ . Recordings were excluded from further analysis if the series resistance or input resistance changed by more than 20% compared to the baseline period. Data were low pass-filtered at 4 kHz and sampled at 10 kHz. NMDAR EPSC peak values were averaged over a 20-ms time window using custom MATLAB 2012a software. All values reported are animal-based values; in cases where multiple cells were recorded from the same animal preparation, the average of cells is presented. All recordings were performed at room temperature.

#### **Quantitative real-time PCR**

For quantitative PCR (qPCR) analysis of rat cortical cultures, cells were harvested at 5, 12, 19, and 26 DIV and RNA was isolated using the Invitrogen PureLink RNA Mini Kit. cDNA was synthesized from RNA transcripts using the iScript Select cDNA Synthesis Kit using Eppendorf Thermocycler. Quantitative real-time PCRs (qRT-PCRs) were performed on a Bio-Rad CFX qRT-PCR machine using iTaq Universal SYBR Green Supermix. Relative expression was calculated using  $\beta$ -actin as a reference gene. Custom primers against rat  $\beta$ -actin (forward: TICAACACCCCAGCCATGT; reverse: GCATACAGGGACAACACACGC; Invitrogen) and rat ZnT1 (forward: TGGGCGCTGACGCTTACT; reverse: GTCAGCCGTGGAGTCAATAGC; Invitrogen) were designed using the National Center for Biotechnology Information Primer-BLAST.

#### Zinc efflux assay

HEK cells were grown in DMEM containing penicillin (100 U/ml), streptomycin (0.1 mg/ml), 2 mM glutamine, and 10% (v/v) fetal calf serum in a 5% CO<sub>2</sub> humidified atmosphere at 37°C. To express ZnT1, HEK293 cells were transfected with ZnT1 or empty plasmid (control) using CaPO<sub>4</sub> precipitation. Briefly,1 μg of mouse ZnT1 (pCMV6, ZnT1; GenBank, Q60738) or empty vector plasmid (pCMV6, OriGene) was incubated with 2 M calcium chloride in Hepes-buffered solution containing 1.5 mM Na<sub>2</sub>HPO<sub>4</sub> to generate a coprecipitate; this solution was then dispersed onto cultured cells for 6 hours. Twenty-four hours later, cells were treated overnight with N2AZ or scN2AZ (3 µM). To visualize intracellular zinc, cells were loaded with the fluorescent zinc indicator FluoZin-3 (2 µM) for 25 min at room temperature before imaging. Cells were imaged using a 480-nm excitation filter and an emission 525-nm long-pass filter on a Zeiss Axiovert 100 inverted microscope with a Polychrome IV monochromator (T.I.L.L. Photonics) and a cooled charge-coupled device camera (PCO). To measure zinc efflux, cells were superfused with Ringer's solution (composition: 120 mM NaCl, 0.8 mM MgCl<sub>2</sub>, 5.4 mM KCl, 1.8 mM CaCl<sub>2</sub>, 20 mM Hepes, and 15 mM glucose), and 1  $\mu$ M Zn<sup>2+</sup> with 5  $\mu$ M pyrithione was added for 150 s. The FluoZin-3 signal was normalized to 10-s baseline in each experiment. Rates of initial decrease of the fluorescent signal following removal of Zn<sup>2+</sup> pyrithione were determined during a 100-s period. For each experiment, at least 30 cells were imaged per coverslip and

rates were averaged for three to five coverslips performed as three independent experiments. Fluorescence imaging measurements were acquired using Axon Imaging Workbench 5.2 (INDEC BioSystems) and analyzed using Excel and Prism GraphPad.

#### Peptide hspot array and far-Western assay

Far-Western protein-binding affinity assays were performed as previously described (25). Peptide spot arrays (15-mers) spanning the proximal C-terminal residues 1390 to 1464 of mouse GluN2A (UniProt no.: P35436) in overlapping one-residue steps were constructed using the Spots-synthesis method. Standard 9-fluorenylmethoxy carbonyl (Fmoc) chemistry was used to synthesize the peptides and spot them onto nitrocellulose membranes, which were prederivatized with a polyethylene glycerol spacer (Intavis). Fmoc-protected and Fmoc-activated amino acids were spotted in 20 to 30 arrays on 150 mm-by-100 mm membranes using an Intavis MultiPep robot. The nitrocellulose membrane containing the immobilized peptides was soaked in *N*-cyclohexyl-3-aminopropanesulfonic acid (CAPS) buffer [10 mM CAPS (pH 11.0) with 20% (v/v) methanol] for 30 min, washed once with tris-buffered 0.1% Tween 20 (TBST), blocked for 1 hour at room temperature with gentle shaking in TBST containing 5% (w/v) nonfat milk, and then incubated with enriched Flag-tagged ZnT1 (SLC30a1) cell lysate (obtained from previously transfected HEK cells) overnight at 4°C with gentle shaking. Next, the membrane was incubated in primary antibody for Flag for 1 hour at room temperature with gentle shaking, followed by washing with TBST. Last, the membrane was incubated in secondary antibody for 45 min, washed three times for 5 min in TBST, and then visualized by infrared fluorescence (Li-Cor). Four independent peptide spot arrays were used in this study. A second set of membranes (n = 4) was treated as above but also in the presence of 100 µM N2AZ or scN2AZ and compared to 0.1% DMSO. For each experiment, an additional peptide array was done with omission of Flag-tagged ZnT1 (SLC30a1) protein to measure and correct for the background due to the primary and secondary antibodies.

#### Statistical analyses

Slice electrophysiology experiments using N2AZ and scN2AZ were completed blind to the identity of the peptide. Experiments in ZnT3 KO and WT animals were completed blind to the genotype. Electrophysiology recordings in cortical cultures and DCN slices were obtained using Ephus software run in MATLAB 2012a (Math-Works). Cell parameters and response peaks were calculated using custom MATLAB scripts. For neuronal culture electrophysiology, ZX1 potentiation was measured as the percent increase in NMDAR amplitude 5 min after the application of ZX1. In slice experiments, ZX1 potentiation was calculated as the average percent increase over baseline of NMDAR or AMPAR EPSCs 10 to 15 min after the addition of ZX1 (Figs. 3, 4, 5, and 6, D to F) or 15 to 20 min after the addition of ZX1 (Fig. 6, A to C). Unpaired t tests and ANOVAs were used to compare between treatments and genotypes. To determine whether ZX1 significantly potentiated responses, paired *t* tests were used to compare amplitude of peak responses before and after addition of ZX1. Statistical analysis was completed in Prism 8 (GraphPad).

#### **SUPPLEMENTARY MATERIALS**

Supplementary material for this article is available at http://advances.sciencemag.org/cgi/content/full/6/27/eabb1515/DC1

View/request a protocol for this paper from Bio-protocol.

#### **REFERENCES AND NOTES**

- K. Vogt, J. Mellor, G. Tong, R. Nicoll, The actions of synaptically released zinc at hippocampal mossy fiber synapses. Neuron 26, 187–196 (2000).
- A. M. Vergnano, N. Rebola, L. P. Savtchenko, P. S. Pinheiro, M. Casado, B. L. Kieffer, D. A. Rusakov, C. Mulle, P. Paoletti, Zinc dynamics and action at excitatory synapses. Neuron 82, 1101–1114 (2014).
- B. I. Kalappa, C. T. Anderson, J. M. Goldberg, S. J. Lippard, T. Tzounopoulos, AMPA receptor inhibition by synaptically released zinc. *Proc. Natl. Acad. Sci. U.S.A.* 112, 15749–15754 (2015).
- C. T. Anderson, R. J. Radford, M. L. Zastrow, D. Y. Zhang, U.-P. Apfel, S. J. Lippard, T. Tzounopoulos, Modulation of extrasynaptic NMDA receptors by synaptic and tonic zinc. Proc. Natl. Acad. Sci. U.S.A. 112, E2705–E2714 (2015).
- K. Hirzel, U. Müller, A. T. Latal, S. Hülsmann, J. Grudzinska, M. W. Seeliger, H. Betz, B. Laube, Hyperekplexia phenotype of glycine receptor α1 subunit mutant mice identifies Zn<sup>2+</sup> as an essential endogenous modulator of glycinergic neurotransmission. *Neuron* 52, 679–690 (2006).
- T. Perez-Rosello, C. T. Anderson, C. Ling, S. J. Lippard, T. Tzounopoulos, Tonic zinc inhibits spontaneous firing in dorsal cochlear nucleus principal neurons by enhancing glycinergic neurotransmission. *Neurobiol. Dis.* 81, 14–19 (2015).
- S. Kouvaros, M. Kumar, T. Tzounopoulos, Synaptic zinc enhances inhibition mediated by somatostatin, but not parvalbumin, cells in mouse auditory cortex. Cereb. Cortex, bhaa005 (2020).
- Y. Z. Huang, E. Pan, Z.-Q. Xiong, J. O. McNamara, Zinc-mediated transactivation of TrkB potentiates the hippocampal mossy fiber-CA3 pyramid synapse. *Neuron* 57, 546–558 (2008).
- E. Pan, X.-A. Zhang, Z. Huang, A. Krezel, M. Zhao, C. E. Tinberg, S. J. Lippard,
  J. O. McNamara, Vesicular zinc promotes presynaptic and inhibits postsynaptic long-term
  potentiation of mossy fiber-CA3 synapse. *Neuron* 71, 1116–1126 (2011).
- K. Eom, J. H. Hyun, D.-G. Lee, S. Kim, H.-J. Jeong, J.-S. Kang, W.-K. Ho, S.-H. Lee, Intracellular Zn<sup>2+</sup> signaling facilitates mossy fiber input-induced heterosynaptic potentiation of direct cortical inputs in hippocampal CA3 pyramidal cells. *J. Neurosci.* 39, 3812–3831 (2019).
- T. Perez-Rosello, C. T. Anderson, F. J. Schopfer, Y. Zhao, D. Gilad, S. R. Salvatore, B. A. Freeman, M. Hershfinkel, E. Aizenman, T. Tzounopoulos, Synaptic Zn<sup>2+</sup> inhibits neurotransmitter release by promoting endocannabinoid synthesis. *J. Neurosci.* 33, 9259–9272 (2013).
- B. I. Kalappa, T. Tzounopoulos, Context-dependent modulation of excitatory synaptic strength by synaptically released zinc. eNeuro 4, ENEURO.0011-0017.2017 (2017).
- C. T. Anderson, M. Kumar, S. Xiong, T. Tzounopoulos, Cell-specific gain modulation by synaptically released zinc in cortical circuits of audition. eLife 6, e29893 (2017).
- H.-P. Patrick Wu, R. H. Dyck, Signaling by synaptic zinc is required for whisker-mediated, fine texture discrimination. *Neuroscience* 369, 242–247 (2018).
- M. Kumar, S. Xiong, T. Tzounopoulos, C. T. Anderson, Fine control of sound frequency tuning and frequency discrimination acuity by synaptic zinc signaling in mouse auditory cortex. J. Neurosci. 39, 854–865 (2019).
- B. B. McAllister, R. H. Dyck, Zinc transporter 3 (ZnT3) and vesicular zinc in central nervous system function. *Neurosci. Biobehav. Rev.* 80, 329–350 (2017).
- S. Y. Assaf, S. H. Chung, Release of endogenous Zn<sup>2+</sup> from brain tissue during activity. Nature 308, 734–736 (1984).
- A. Ruiz, M. C. Walker, R. Fabian-Fine, D. M. Kullmann, Endogenous zinc inhibits GABA<sub>A</sub> receptors in a hippocampal pathway. J. Neurophysiol. 91, 1091–1096 (2004).
- L. Besser, E. Chorin, I. Sekler, W. F. Silverman, S. Atkin, J. T. Russell, M. Hershfinkel, Synaptically released zinc triggers metabotropic signaling via a zinc-sensing receptor in the hippocampus. *J. Neurosci.* 29, 2890–2901 (2009).
- P. Paoletti, P. Ascher, J. Neyton, High-affinity zinc inhibition of NMDA NR1-NR2A receptors. J. Neurosci. 17, 5711–5725 (1997).
- T. Kambe, A. Hashimoto, S. Fujimoto, Current understanding of ZIP and ZnT zinc transporters in human health and diseases. Cell. Mol. Life Sci. 71, 3281–3295 (2014).
- C. Sindreu, Á. Bayés, X. Altafaj, J. Pérez-Clausell, Zinc transporter-1 concentrates at the postsynaptic density of hippocampal synapses. Mol. Brain 7, 16 (2014).
- M. Mellone, S. Pelucchi, L. Alberti, A. A. Genazzani, M. D. Luca, F. Gardoni, Zinc transporter-1: A novel NMDA receptor-binding protein at the postsynaptic density. *J. Neurochem.* 132, 159–168 (2015).
- J. M. Brittain, L. Chen, S. M. Wilson, T. Brustovetsky, X. Gao, N. M. Ashpole, A. I. Molosh, H. You, A. Hudmon, A. Shekhar, F. A. White, G. W. Zamponi, N. Brustovetsky, J. Chen, R. Khanna, Neuroprotection against traumatic brain injury by a peptide derived from the collapsin response mediator protein 2 (CRMP2). *J. Biol. Chem.* 286, 37778–37792 (2011).
- C. Y. Yeh, A. M. Bulas, A. Moutal, J. L. Saloman, K. A. Hartnett, C. T. Anderson,
   T. Tzounopoulos, D. Sun, R. Khanna, E. Aizenman, Targeting a potassium channel/syntaxin interaction ameliorates cell death in ischemic stroke. *J. Neurosci.* 37, 5648–5658 (2017).
- J. D. Sinor, S. Du, S. Venneti, R. C. Blitzblau, D. N. Leszkiewicz, P. A. Rosenberg,
   E. Aizenman, NMDA and glutamate evoke excitotoxicity at distinct cellular locations in rat cortical neurons in vitro. J. Neurosci. 20, 8831–8837 (2000).

#### SCIENCE ADVANCES | RESEARCH ARTICLE

- X. Zhu, A. Zelmer, S. Wellmann, Visualization of protein-protein interaction in nuclear and cytoplasmic fractions by co-immunoprecipitation and in situ proximity ligation assay. J. Vis. Exp., 55218 (2017).
- E. Shusterman, O. Beharier, L. Shiri, R. Zarivach, Y. Etzion, C. R. Campbell, I.-H. Lee, K. Okabayashi, A. Dinudom, D. I. Cook, A. Katz, A. Moran, ZnT-1 extrudes zinc from mammalian cells functioning as a Zn<sup>2+</sup>/H<sup>+</sup> exchanger. Metallomics 6, 1656–1663 (2014).
- 29. C. J. Frederickson, G. A. Howell, M. D. Haigh, G. Danscher, Zinc-containing fiber systems in the cochlear nuclei of the rat and mouse. *Hear. Res.* **36**, 203–211 (1988).
- J. Bialecki, A. Werner, N. L. Weilinger, C. M. Tucker, H. A. Vecchiarelli, J. Egaña, J. Mendizabal-Zubiaga, P. Grandes, M. N. Hill, R. J. Thompson, Suppression of presynaptic glutamate release by postsynaptic metabotropic NMDA receptor signalling to pannexin-1. J. Neurosci. 40, 729–742 (2020).
- J. H. Weiss, D. M. Hartley, J. Y. Koh, D. W. Choi, AMPA receptor activation potentiates zinc neurotoxicity. *Neuron* 10. 43–49 (1993).
- G. A. Kerchner, L. M. Canzoniero, S. P. Yu, C. Ling, D. W. Choi, Zn<sup>2+</sup> current is mediated by voltage-gated Ca<sup>2+</sup> channels and enhanced by extracellular acidity in mouse cortical neurones. *J. Physiol.* **528**, 39–52 (2000).
- E. Shusterman, O. Beharier, S. Levy, R. Zarivach, Y. Etzion, C. R. Campbell, I.-H. Lee, A. Dinudom, D. I. Cook, A. Peretz, A. Katz, D. Gitler, A. Moran, Zinc transport and the inhibition of the L-type calcium channel are two separable functions of ZnT-1. *Metallomics* 9, 228–238 (2017).
- M. J. Berridge, Calcium microdomains: Organization and function. Cell Calcium 40, 405–412 (2006).
- P. Paoletti, A. M. Vergnano, B. Barbour, M. Casado, Zinc at glutamatergic synapses. Neuroscience 158, 126–136 (2009).
- M. Hershfinkel, A. Moran, N. Grossman, I. Sekler, A zinc-sensing receptor triggers the release of intracellular Ca<sup>2+</sup> and regulates ion transport. *Proc. Natl. Acad. Sci. U.S.A.* 98, 11749–11754 (2001).
- N. Lavoie, D. V. Jeyaraju, M. R. Peralta III, L. Seress, L. Pellegrini, K. Tóth, Vesicular zinc regulates the Ca<sup>2+</sup> sensitivity of a subpopulation of presynaptic vesicles at hippocampal mossy fiber terminals. *J. Neurosci.* 31, 18251–18265 (2011).
- H. J. Wenzel, T. B. Cole, D. E. Born, P. A. Schwartzkroin, R. D. Palmiter, Ultrastructural localization of zinc transporter-3 (ZnT-3) to synaptic vesicle membranes within mossy fiber boutons in the hippocampus of mouse and monkey. *Proc. Natl. Acad. Sci. U.S.A.* 94, 12676–12681 (1997).
- M. E. Quinta-Ferreira, C. M. Matias, Tetanically released zinc inhibits hippocampal mossy fiber calcium. zinc and synaptic responses. *Brain Res.* 1047. 1–9 (2005).
- S. G. Cull-Candy, D. N. Leszkiewicz, Role of distinct NMDA receptor subtypes at central synapses. Sci. STKE 2004, re16 (2004).
- M. P. Parsons, L. A. Raymond, Extrasynaptic NMDA receptor involvement in central nervous system disorders. *Neuron* 82: 279–293 (2014).
- Y. Nishito, T. Kambe, Zinc transporter 1 (ZNT1) expression on the cell surface is elaborately controlled by cellular zinc levels. J. Biol. Chem. 294, 15686–15697 (2019).
- J. E. J. Hardyman, J. Tyson, K. A. Jackson, C. Aldridge, S. J. Cockell, L. A. Wakeling,
   R. A. Valentine, D. Ford, Zinc sensing by metal-responsive transcription factor 1 (MTF1)

- controls metallothionein and ZnT1 expression to buffer the sensitivity of the transcriptome response to zinc. *Metallomics* **8**, 337–343 (2016).
- C. T. Sheline, H. S. Ying, C. S. Ling, L. M. T. Canzoniero, D. W. Choi, Depolarization-induced <sup>65</sup>zinc influx into cultured cortical neurons. *Neurobiol. Dis.* 10, 41–53 (2002).
- E. Aizenman, A. K. Stout, K. A. Hartnett, K. E. Dineley, B. McLaughlin, I. J. Reynolds, Induction of neuronal apoptosis by thiol oxidation: Putative role of intracellular zinc release. J. Neurochem. 75, 1878–1888 (2000).
- T. A. Vander Jagt, J. A. Connor, J. H. Weiss, C. W. Shuttleworth, Intracellular Zn<sup>2+</sup> increases contribute to the progression of excitotoxic Ca<sup>2+</sup> increases in apical dendrites of CA1 pyramidal neurons. *Neuroscience* 159, 104–114 (2009).
- I. J. Reynolds, T. G. Hastings, Glutamate induces the production of reactive oxygen species in cultured forebrain neurons following NMDA receptor activation. *J. Neurosci.* 15, 3318–3327 (1995).
- J. Qian, K. Xu, J. Yoo, T. T. Chen, G. Andrews, J. L. Noebels, Knockout of Zn transporters Zip-1 and Zip-3 attenuates seizure-induced CA1 neurodegeneration. J. Neurosci. 31, 97–104 (2011).
- P. A. Rosenberg, E. Aizenman, Hundred-fold increase in neuronal vulnerability to glutamate toxicity in astrocyte-poor cultures of rat cerebral cortex. *Neurosci. Lett.* 103, 162–168 (1989)
- T. Tzounopoulos, Y. Kim, D. Oertel, L. O. Trussell, Cell-specific, spike timing-dependent plasticities in the dorsal cochlear nucleus. *Nat. Neurosci.* 7, 719–725 (2004).

Acknowledgments: We thank C. Anderson for technical help with MATLAB and discussions and K. Hartnett-Scott for technical assistance. Funding: This work was supported by NSF grant NSF-IOS-BSF 1655480 (to E.A., T.T., and M.H.) and NIH grants DC007905 (to T.T.), NS043277 (to E.A.), GM128195 (to J.W.J.), and F31 NS1134477 (to M.B.P.). Author contributions: R.F.K., E.A., T.T., A.M., R.K., H.A., M.H., M.B.P., and J.W.J. designed experiments. R.F.K., E.A., and M.B.P. conducted experiments and performed data analysis. R.F.K., E.A., and T.T. wrote the manuscript. Competing interests: A provisional patent application entitled "Peptides that enhance NMDA receptor function and use thereof," application no. 62/942,979, was filed on 3 December 2019 (assignee: University of Pittsburgh; co-inventors: E.A. and T.T.). The authors declare no other competing interests. Data and materials availability: All data needed to evaluate the conclusions in the paper are present in the paper and/or the Supplementary Materials. Additional data related to this paper may be requested from the authors.

Submitted 4 February 2020 Accepted 20 May 2020 Published 3 July 2020 10.1126/sciadv.abb1515

Citation: R. F. Krall, A. Moutal, M. B. Phillips, H. Asraf, J. W. Johnson, R. Khanna, M. Hershfinkel, E. Aizenman, T. Tzounopoulos, Synaptic zinc inhibition of NMDA receptors depends on the association of GluN2A with the zinc transporter ZnT1. Sci. Adv. 6. eabb1515 (2020).

# **Science** Advances

# Synaptic zinc inhibition of NMDA receptors depends on the association of GluN2A with the zinc transporter ZnT1

Rebecca F. Krall, Aubin Moutal, Matthew B. Phillips, Hila Asraf, Jon W. Johnson, Rajesh Khanna, Michal Hershfinkel, Elias Aizenman, and Thanos Tzounopoulos

Sci. Adv., **6** (27), eabb1515. DOI: 10.1126/sciadv.abb1515

View the article online

https://www.science.org/doi/10.1126/sciadv.abb1515

**Permissions** 

https://www.science.org/help/reprints-and-permissions

Use of this article is subject to the Terms of service